AIAA JOURNAL
Vol. 44, No. 7, July 2006

Approximate Spectral Element for Wave Propagation Analysis in Inhomogeneous Layered Media

A. Chakraborty* and S. Gopalakrishnan†
Indian Institute of Science, Bangalore 560 012, India

An approximate spectral element (SE) is developed to model isotropic inhomogeneous layered media. As opposed to the case of a homogeneous solid, where the mass distribution is modeled exactly, the SE approach to the inhomogeneous material gives an approximate frequency response of the structure. The element is formulated by approximating wave number over the domain. This wave number has a nontrivial imaginary part justifying the notion of an inhomogeneous wave, which is predominant in inhomogeneous materials. Material properties are made to vary linearly within the element, although any other variation can be incorporated under the proposed scheme. Strains due to temperature are also taken into account, which enables the analysis of a layered structure for thermal burst loading. The formulated element is used to analyze the response of inhomogeneous layer structure subjected to high-frequency mechanical and thermal loading. Furthermore, the inherent advantage of the SE in the solution of inverse problems is utilized to reconstruct the force history applied to an inhomogeneous layer from the measured responses. The finite element responses are used as surrogate experimental data. In particular, a layered structure of functionally graded material (FGM) is taken for the case study, where FGM smoothly blends two different material properties, one of metal and the other of ceramic. The fast Fourier transform and Fourier series are used for inversion to the time/space domain.

Nomenclature

$\boldsymbol{E}$	=	Green–Lagrange strain tensor
k, η	=	vertical and horizontal wave numbers
L	=	element length in x direction
$\boldsymbol{T}$	=	Cauchey stress tensor
t	=	time coordinate
$\boldsymbol{u}(\bar{\boldsymbol{x}}, t)$	=	displacement vector
$\bar{\boldsymbol{x}}$	=	spatial coordinate vector with components (x, y)
Y, T	=	spatial and temporal time windows
α, β, γ	=	inhomogeneous parameters
α_x, α_y	=	coefficient of thermal expansion in x and y directions
ΔT	=	temperature rise/fall
δ_{ij}	=	Kronecker delta
$\lambda(\bar{\boldsymbol{x}}), \mu(\bar{\boldsymbol{x}})$	=	Lame's constants
$\rho(\boldsymbol{x})$	=	density
ω	=	circular frequency

Introduction

WAVE propagation in linear homogeneous and nondissipative solid can be described by a homogeneous plane wave solution of the form $\boldsymbol{u} = \boldsymbol{A}\exp[j(\boldsymbol{k}\cdot\boldsymbol{x} - \omega t)]$, $j^2 = -1$, where $\boldsymbol{A}$ and $\boldsymbol{k}$ are real. $\boldsymbol{A}$ is the wave amplitude, and $\boldsymbol{k}$ is the wave vector. However, if the material sustaining wave propagation is (linear and) dissipative, the simplest wave will be of the preceding form with complex $\boldsymbol{A}$ and $\boldsymbol{k}$. Such waves are called inhomogeneous waves.[1] The most common media that exhibit inhomogeneous waves are those with inbuilt dissipative properties such as viscoelastic materials. It is known that time-harmonic waves in dissipative media have a complex-valued wave number. However, it is less known that there can be waves with a complex-valued wave vector, with real and imaginary parts $\boldsymbol{k}_1$ and $\boldsymbol{k}_2$ not necessary parallel.[2] Thus, more precisely, inhomogeneous waves are the waves where the wave vector $\boldsymbol{k}$ is complex valued and is of the form $\boldsymbol{k} = \boldsymbol{k}_1 + j\boldsymbol{k}_2$.

Other materials exhibiting this wave behavior are those whose elastic and inertial properties vary continuously in spatial directions. In practice, all materials are of this type, and we make an approximation by considering them as homogeneous. Earlier, industrial materials and metals were necessarily homogeneous barring their flaws. Presently, there is a trend to manufacture inhomogeneous materials, artificially, having desired variation of material properties in spatial directions. These are the functionally graded materials (FGM), and their extensive use in different fields such as aerospace, defense, and automobile industries demand accurate behavior prediction of these materials. Requirements of these materials originate from different service requirements demanded from conventional materials, which in most cases conventional materials fail to provide. Present day applications demand the use of more than one kind of materials (such as ceramic for toughness and thermal insulation and metal for strength and ductility). The problem occurs at the interface of these two materials, where failure may occur due to stress jump (because of the large mismatch in elastic modulus) or residual stress (because of the mismatch in coefficient of thermal expansion). This situation is greatly improved by the use of FGM at the bimaterial interface. Instead of an abrupt jump, material properties in FGM gradually vary from one material to another in discrete steps. FGM is essentially made up of as a mixture of ceramic and steel, and this gradation is achieved by varying the volume fraction of the metal or ceramic from 100 to 0% in several steps.

Wave propagation analysis of FGM poses a tremendous challenge because of the material inhomogeneity. The literature on the response of this material to high-frequency impact loading is limited in number, and these few works mostly deal with FGM plates and cylinders. The earliest works reported on wave propagation in a FGM plate are those of Liu et al.[3,4] and Liu and Tani.[5,6] Reddy and Chin[7] and Praveen and Reddy[8] analyzed FGM plates and cylinders taking thermal stress into consideration. Furthermore, Gong et al.[9] analyzed an FGM shell for wave propagation due to low-velocity impact. Recently, there have been a few works that deal with issues related to wave propagation in FGM by numerical domain transfer approach,[10] hybrid numerical method,[11] and analytical–numerical

Presented as Paper 2003-1590 at the AIAA/ASME/ASCE/AHS 44th Structures, Structural Dynamics, and Materials Conference, Norfolk, VA, 7–10 April 2003; received 5 August 2003; revision received 14 November 2005; accepted for publication 10 January 2006.

*Graduate Student, Department of Aerospace Engineering. Member AIAA.

†Assistant Professor, Department of Aerospace Engineering; Krishnan@aero.iisc.ernet.in.

approach.[12] More recently, Chakraborty and Gopalakrishnan,[13,14] addressed wave propagation in FGM directly using the exact beam finite element (FE) and spectral element (SE) approaches.

There is a marked difference between the previously reported works and the present work. In all of the cited cases, it is assumed that material properties do not vary in the direction of wave propagation. This assumption greatly simplifies the analysis, and it must be mentioned that there will not be any difference in the computational scheme with that taken for composite material analysis. Once the depthwise integrated material constants ($\boldsymbol{A}$, $\boldsymbol{B}$, and $\boldsymbol{D}$ matrices) are obtained (in a different way for composites and FGM) the remainder of the procedure remains essentially same for composites and FGM. Moreover, the assumption acts as a hindrance to recognize the inhomogeneous nature of the wave.

Mathematically, a plane wave solution does not exist for inhomogeneous materials[1] where approximate techniques need to be employed. These techniques essentially consider the inhomogeneous material as a perturbation to the inhomogeneous material, and the Born approximation, Wentzel–Kramers–Brillouin–Jeffreys (WKBJ) approximation, etc., are employed. However, the notion of wave number still can be retained in a local sense. The first work that considered wave propagation in the direction of the material property variation is that of Chakraborty and Gopalakrishnan,[15] where a one-dimensional waveguide is considered with lengthwise material property variation. It is shown in that paper how an approximate wave number can be derived for inhomogeneous materials, where the wave number contains a nontrivial imaginary part, which acts to attenuate the wave amplitudes. Nevertheless, the wave generated in one-dimensional structure is a synthesis of wave numbers rather than wave vectors and, rigorously, that wave cannot be called inhomogeneous wave. In this respect, the present work is most suitable to capture an inhomogeneous wave because more than one spatial dimension is involved. Here, it will be shown how an approximate plane wave solution can be obtained using an approximate wave vector. The main difficulty arises due to the nature of the governing equation, which instead of being an equation with constant coefficients (homogeneous material), the inhomogeneity gives rise to a partial differential equation with variable coefficients. This equation needs to be solved in frequency/wave vector domain, which is in the realm of spectral analysis.

The spectral analysis[16] has established itself as arguably the most powerful method for wave propagation analysis. An impact load, which triggers wave propagation, has high-frequency content. Thus, the load excites numerous modes of the structure. An analysis of this problem, using mode superposition or other reduction techniques, becomes a futile exercise because it is computationally too expensive to perform eigenanalysis for extracting a large number of eigenvalues/vectors that are to be used subsequently for response estimation. The SE method circumvents this problem in a most elegant way. The formulation for one/two-dimensional structure begins by transforming the governing elastodynamic equation in the frequency domain. The transformed equation loses one independent variable, that is, time. (Frequency comes as a parameter.) For a one-dimensional structure, the reduced equation is an ordinary differential equation (ODE), which is to be solved. For homogeneous material, this ODE can be solved exactly, and the exact solution is used to formulate SEs by following the normal procedures of FE analysis. However, for a two-dimensional structure, the reduced equation is still a partial differential equation (PDE) of two independent (spatial) variables, and further transformation is necessary. This is achieved by transforming the equation in wave vector domain. For homogeneous materials, this transformation is justified because the PDE is of constant coefficients. The transformed equation forms an algebraic relation between applied force and unknown displacements, which results in the formulation of the layered SE.

The layered SE for homogeneous material was developed by Rizzi and Doyle.[17] They solved the governing Navier's equation using Helmholtz decomposition of the displacement field. Solutions were obtained by summing a generic kernel (solution) function over many discrete frequency and wave number components. For inhomogeneous layers, there are only two works so far that dealt with wave propagation. Han and Liu[18] formulated a layer element for horizontal shear wave propagation, which allows quadratic variation of material properties through the depth. The element is formulated by exactly solving the governing equation, which was possible for the quadratic form of the variation. In a work by Berezovski et al.,[19] propagation of stress waves through the FGM layer is studied, where the layer can have randomly embedded ceramic particles in the metal with a prescribed volume fraction, and a wave propagation algorithm is used.

In the present work, Navier's equation for inhomogeneous material is solved assuming a wave-type solution, and the dispersion relation is obtained approximately for the wave vectors, resulting an approximate two-nodded SE, which is bounded only in one direction. Note that a single element is sufficient to model a heterogeneous layer in this approach when the order of nonhomogeneity is not too high. Here, the power law [for a Voight-type estimate (see Ref. 20)] is assumed for material property variation in the FGM layer. In particular, the value of the exponent is taken as unity, that is, linear variation is considered. The main requirement of using FGM is smoothening of stresses in bimaterial interfaces. This aspect is studied in the numerical section. One major difficulty associated with the use of an FGM material is the generation of small pockets of residual stresses in the layer because of the mismatch in coefficient of thermal expansion of the base materials. As a prelude to the detailed study of the residual stresses, the element is formulated with the provision for thermal analysis. Strain due to temperature is also taken into account, and the layer is analyzed to obtain the responses of thermal burst loading.

Another important issue related to inhomogeneous material is solving inverse problems, in particular, material and force identification. Although there are few new papers on material identification of FGM layer, to the authors' best knowledge, very few works are reported on force identification. The present element is suitable for force identification because the frequency response function is the direct byproduct of the spectral approach. The convenience and versatility of SE in conjunction with experimental data has been previously demonstrated to predict force in monomaterial beam,[21] bimaterial beam,[22] isotropic plates,[23] orthotropic plates,[24] and layered media.[16] In all of the mentioned works, experimentally generated responses of the structure were fed in the SE solver, which produced the required force as output.

There are instances where it is difficult to obtain a suitable physical model for impact testing, and under these circumstances, simulation becomes necessary. Also, several difficulties are associated with wave propagation experiments performed over a finite length models in terms of noises and boundary reflections. For effective force identification, a complete trace of the measured signal is required. The experimentally generated signal needs to be truncated at some point. Choosing the point of truncation requires critical consideration because one may loose information by truncating the signal prematurely. For a dispersive system, in particular, caution should be exercised in selection of this truncation point because the wave response will not die down completely within the chosen time window. In this work, the FE analysis results are used as surrogate experiment results. Because experimental outputs are always truncated at some point, depending on constraints of the setup, data acquisition system, and other facilities, the FE response should be taken such that it simulates the experimental results. When this truncated response is given as input to the SE solver, the force data can be reconstructed by performing inverse analysis. This idea is explored in this work to identify the impact forces applied in inhomogeneous layer media.

In the next section, the formulation of the SE is outlined in detail, where the effect of thermal strain is also considered. The formulated element is validated next. Smoothening of response and stresses by FGM is demonstrated next. This is followed by one example involving a thermal burst loading, where the response and stress behaviors are studied. Finally, solution of the inverse problem in terms of force reconstruction is demonstrated.

Mathematical Model

The elastodynamic equation of motion for a general inhomogeneous isotropic material is

$$\nabla \cdot \boldsymbol{T} = \rho(\bar{\boldsymbol{x}})\ddot{u}(\bar{\boldsymbol{x}}, t) \tag{1}$$

where the overdot denotes differentiation with respect to time. $\boldsymbol{T}$ is related to $\boldsymbol{E}$ by

$$\boldsymbol{T} = 2\mu(\bar{\boldsymbol{x}})\boldsymbol{E} + \lambda(\bar{\boldsymbol{x}})\,\mathrm{tr}(\boldsymbol{E})\delta_{ij} \tag{2}$$

where tr( ) denotes trace of a matrix. $\boldsymbol{E}$ is related to $\boldsymbol{u}(\bar{\boldsymbol{x}}, t)$ by

$$\boldsymbol{E} = \left(\tfrac{1}{2}\right)(\nabla \boldsymbol{u} + \nabla \boldsymbol{u}^t) \tag{3}$$

where t in the superscript denotes the transpose of a vector or a matrix. When Eqs. (3) and (2) are substituted in Eq. (1), the expanded form of the governing equation is

$$\rho(\bar{\boldsymbol{x}})\ddot{\boldsymbol{u}}(\bar{\boldsymbol{x}}, t) = \nabla \cdot \left[\mu(\nabla \boldsymbol{u} + \nabla \boldsymbol{u}^t) + \lambda(\nabla \cdot \boldsymbol{u})\delta_{ij}\right] = \mu\nabla^2 \boldsymbol{u}$$

$$+ (\mu + \lambda)\nabla(\nabla \cdot \boldsymbol{u}) + \nabla\mu(\nabla \boldsymbol{u} + \nabla \boldsymbol{u}^t) + \nabla\lambda(\nabla \cdot \boldsymbol{u}) \tag{4}$$

In the present case, two-dimensional Euclidean space $[\bar{\boldsymbol{x}} = (x, y)]$ is considered, and relevant stresses and strains are T_{11}, T_{12}, T_{22}, and E_{11}, E_{12}, and E_{22}, respectively. Also, it is assumed that the material properties are varying only in the layer direction x in a linear fashion (Fig. 1) as

$$\lambda(x, y) = \lambda_0(1 + \alpha x), \qquad \mu(x, y) = \mu_0(1 + \beta x)$$

$$\rho(x, y) = \rho_0(1 + \gamma x) \tag{5}$$

where λ_0, μ_0, and ρ_0 are values of the respective properties at some reference point, for example, $x = 0$, and α, β, and γ are rates of change of those properties in spatial coordinates. When a time-harmonic solution is assumed, the displacement field can be written as

$$\boldsymbol{u}(\bar{\boldsymbol{x}}, t) = \hat{\boldsymbol{u}}(\bar{\boldsymbol{x}})e^{-j\omega t} \tag{7}$$

The displacement field $\boldsymbol{u}$ has components u and v in the x and y directions, respectively. We further assume that spatial dependence of u and v in the y direction can be obtained by summing cosine or sine functions over many discrete horizontal wave numbers.

The spectral form of the displacement field can now be written in terms of a double Fourier series as

$$u = \sum_{n=1}^{N-1}\sum_{m=1}^{M-1} \hat{u}(x, \eta_m, \omega_n) \left\{ \begin{matrix} \cos(\eta_m, y) \\ \sin(\eta_m, y) \end{matrix} \right\} e^{-j\omega_n t}$$

$$v = \sum_{n=1}^{N-1}\sum_{m=1}^{M-1} \hat{v}(x, \eta_m, \omega_n) \left\{ \begin{matrix} \cos(\eta_m, y) \\ \sin(\eta_m, y) \end{matrix} \right\} e^{-j\omega_n t}$$

where N and M are to be chosen based on criteria dictated by length of time and space window required. The y dependency is chosen based on a symmetric (cosine) or antisymmetric (sine) loading condition. In all subsequent formulations, only the symmetric loading (about $y = 0$) is considered.

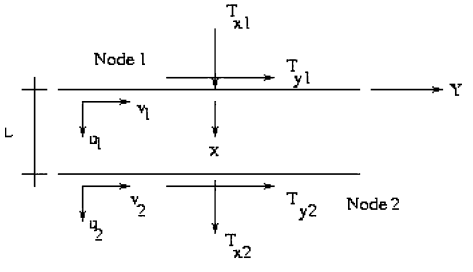

Fig. 1 Two-noded layered SE and degrees of freedom.

Spectrum Relation

As is normally done for homogeneous material, the x dependency of the displacement field for inhomogeneous material is naively assumed as

$$\hat{\boldsymbol{u}}(x, \eta_m, \omega_n) = \tilde{\boldsymbol{u}} \exp[-jk(\eta_m, \omega_n, x)x] \tag{8}$$

The condition on the values of wave number $k(\eta_m, \omega_n, x)$, that is, k_{mn}, can be found by substituting the preceding field in the governing equation, where it is assumed that $\partial k/\partial x$ is negligible. This is the key assumption in the present formulation, and its behavior over a homogeneous wave number in a one-dimensional case has been shown.[13] The expectation is that, even in two dimensions, because we are essentially dealing with a wave number in one particular direction (where the other direction is infinite), this approximation will yield a better result compared to any layerwise constant material property assumptions. When the assumed displacement field is substituted in Eq. (4), the governing differential equation is converted to an algebraic (matrix–vector) equation of the form

$$[\boldsymbol{W}]\{\tilde{\boldsymbol{u}}\} = \boldsymbol{0} \tag{9}$$

The elements of the wave matrix $[\boldsymbol{W}]$ (2×2) (where k and η are k_{mn} and η_m, respectively) are

$$W_{11} = -2j\alpha\mu k - 2\mu k^2 - j\beta\lambda k - \lambda k^2 - \mu\eta^2 + \rho\omega^2$$

$$W_{12} = \beta\lambda\eta - j\lambda k\eta - j\mu k\eta, \qquad W_{21} = -\alpha\mu\eta + j\lambda k\eta + j\mu k\eta$$

$$W_{22} = -\mu k^2 - 2\mu\eta^2 - j\alpha\mu k - \lambda\eta^2 + \rho\omega^2$$

where λ, μ, and ρ are all functions of x. For the nontrivial solution of $\tilde{\boldsymbol{u}}$, $[\boldsymbol{W}]$ should be singular and $\tilde{\boldsymbol{u}}$ will be in the null space of $[\boldsymbol{W}]$. The described conditions give the required equations to find the wave numbers k_{mn} and null vectors $\tilde{\boldsymbol{u}}$. To make the wave matrix singular, its determinant should be zero, which in this case is a polynomial equation, whose roots are the wave numbers k_{mn}. The characteristic equation (also called the spectrum relation) is given by

$$(\lambda + 2\mu)\mu k^4 + j(4\alpha\mu^2 + \beta\lambda\mu + \lambda\alpha\mu)k^3$$

$$+ (-3\mu\rho\omega^2 + 2\mu\lambda\eta^2 - \lambda\rho\omega^2 - \beta\alpha\lambda\mu - 2\alpha^2\mu^2 + 4\mu^2\eta^2)k^2$$

$$+ j(-3\alpha\mu\rho\omega^2 + 4\alpha\mu^2\eta^2 + \beta\lambda\mu\eta^2 - \beta\lambda\rho\omega^2 + \alpha\mu\lambda\eta^2)k$$

$$- 3\mu\eta^2\rho\omega^2 + \rho^2\omega^4 + \mu\eta^4\lambda + \beta\eta^2\alpha\lambda\mu - \rho\omega^2\lambda\eta^2$$

$$+ 2\mu^2\eta^4 = 0$$

where k stands for k_{mn}. The equation is fourth-order polynomial with complex coefficients. The equation is a perturbed form of the spectrum relation of any homogeneous isotropic layer, where the coefficients of k^3 and k are zero. Here, although the coefficients are not zero, their magnitude is less than the other three coefficients. The roots, as a consequence, will not be a pair of complex conjugates but a perturbed form of the roots of isotropic homogeneous materials. For this equation, closed-form solutions for all four roots are not available. The situation is further complicated by the fact that the coefficients are functions of x and that a solution containing x as a parameter is precluded. Instead, the equation can be solved numerically for each value of x, which will make the equation one with constant coefficients. In particular, the coefficients can be computed at some representative point (middepth $x = L/2$ here) in the layer. The equation has four complex roots, which are to be solved for each value of ω_n and η_m. The equation is solved by computing the eigenvalues of the companion form of this polynomial, where LAPACK subroutines are used for computation. The root finding method has a direct bearing on the computation of null spaces. In the one-dimensional case, it is possible to solve for one particular root at a time and calculate rest of the roots in terms of the first. In this way, root tracking is performed, and computations of null vectors $\tilde{\boldsymbol{u}}$ can be done by explicit formulation, which depends on the wave numbers.[12]

Such an approach could not be adopted here. In the present case, because all roots are computed at the same time, it is not possible to keep track of any specific root, and a different kind of algorithm is necessary to compute the null vectors $\tilde{\boldsymbol{u}}$. Because $\tilde{\boldsymbol{u}}$ lies in the null space of $[\boldsymbol{W}]$, we have to know the basis of the null space of $[\boldsymbol{W}]$. The basis vectors of the null space can be computed by singular value decomposition (SVD) of the wave matrix $[\boldsymbol{W}]$, that is, $[\boldsymbol{W}] = [\boldsymbol{U}][\boldsymbol{S}][\boldsymbol{V}]^t$, where $[S]$ contains the singular values of $[\boldsymbol{W}]$ and here the transpose indicates Hermitian conjugate. The columns of $[V]$ that correspond to zero singular values form an orthonormal basis for the null space of $[\boldsymbol{W}]$. Efficient SVD subroutines such as that of LAPACK are employed to compute the basis vectors, which performs recursive operation $4 \times (M-1) \times (N-1)$ times. Because all we need are elements of the null space of $[\boldsymbol{W}]$, we can also take the basis vectors themselves and, thus, can provide a simple form to the wave amplitude matrix (dealt in next section). This method of finding roots and null vectors is sufficiently accurate and fast, which is absolutely necessary because of repeated evaluation in one run, that is, $(M-1) \times (N-1)$ times.

Finite-Depth SE

Once the wave numbers and basis vectors of the null space are calculated, they can be used to express the x dependency of the displacement field. First, a two-noded layered SE formulation is considered, which is bounded only in x direction. The SE has two degrees of freedom at each node and tractions are specified at the nodes instead of forces (Fig. 1).

The displacement field can be written as

$$\hat{u}(x) = R_{11}Ae^{-jk_1x} + R_{12}Be^{-jk_2x} + R_{13}Ce^{-jk_3x} + R_{14}Be^{-jk_4x}$$

$$\hat{v}(x) = R_{21}Ae^{-jk_1x} + R_{22}Be^{-jk_2x} + R_{23}Ce^{-jk_3x} + R_{24}Be^{-jk_4x}$$

or in compact form

$$\hat{\boldsymbol{u}} = [\boldsymbol{R}][\Lambda(x)]\{\boldsymbol{a}\} \tag{10}$$

where $[\boldsymbol{R}]$ is the wave amplitude matrix containing the earlier computed basis vectors as column vectors and $[\Lambda(x)]$ is a diagonal matrix containing e^{-jk_ix}, $i = 1, \ldots, 4$. The $\{\boldsymbol{a}\}$ is the vector of unknown constants A, B, C, and D, which again can be written in terms of unknown nodal displacements $\hat{u}(0)$, $\hat{u}(L)$, $\hat{v}(0)$, and $\hat{v}(L)$ by evaluating the displacements at the two nodes. The relation can be written as

$$\tilde{\boldsymbol{u}} = [\boldsymbol{S}]\ \{\boldsymbol{a}\} \tag{11}$$

where $\tilde{\boldsymbol{u}}$ is the vector of nodal displacements. Elements of the matrix $[\boldsymbol{S}]$ can be written in terms of elements of $[\boldsymbol{R}]$ as

$$\boldsymbol{S} = \begin{bmatrix} R_{11} & R_{12} & R_{13} & R_{14} \\ R_{21} & R_{22} & R_{23} & R_{24} \\ R_{11}x_1 & R_{12}x_2 & R_{13}x_3 & R_{14}x_4 \\ R_{21}x_1 & R_{22}x_2 & R_{23}x_3 & R_{24}x_4 \end{bmatrix} \tag{12}$$

where $x_l = e^{-jk_lx}$, $l = 1, \cdots, 4$. At the nodes, surface tractions are specified. Because the surface normal vectors has components $n_x = \mp 1$ and $n_y = 0$, at node 1 and node 2, surface tractions t_x and t_y are related to the stresses by

$$T_{x1} = -T_{11}(0), \qquad T_{x2} = T_{11}(L)$$

$$T_{y1} = -T_{12}(0), \qquad T_{y2} = T_{12}(L) \tag{13}$$

The stresses are related to strains by Eq. (2), where Lame's parameters are functions of x only. Hence, at nodes 1 and 2, which have x coordinate 0 and L, respectively, stresses are related to strains by

$$T_{11}(0) = (\lambda_0 + 2\mu_0)E_{11}(0) + \lambda_0 E_{22}(0)$$

$$T_{11}(L) = (\lambda_L + 2\mu_L)E_{11}(L) + \lambda_L E_{22}(L)$$

$$T_{12}(0) = \mu_0 E_{12}(0), \qquad T_{12}(L) = \mu_L E_{12}(L)$$

where $\lambda_L = \lambda_0(1 + \alpha L)$ and $\mu_L = \mu_0(1 + \beta L)$.

When the preceding equations and the assumed form of the displacement field Eq. (10) is substituted in Eq. (13), nodal surface tractions can be written in terms of unknown coefficients and, in turn, in terms of nodal displacements as

$$\{\boldsymbol{t}\} = [\boldsymbol{P}]\{\boldsymbol{a}\}, \qquad \{\boldsymbol{t}\} = \{T_{x1}, T_{y1}, T_{x2}, T_{y2}\}^T \tag{14}$$

where the superscript T denotes the transpose of the vector.

The elements of $[\boldsymbol{P}]$ are

$$P_{1p} = j(2\mu + \lambda)R_{1p}k_p - \lambda\eta R_{2p}$$

$$P_{2p} = -\mu(-jR_{2p}k_p - \eta R_{1p})$$

$$P_{3p} = -j(2\mu + \lambda)R_{1p}k_px_p + \lambda\eta R_{2p}x_p$$

$$P_{4p} = \mu(-jR_{2p}k_p - \eta R_{1p})x_p \tag{15}$$

where p varies from 1 to 4 and x_p is as defined earlier.

When Eq. (11) is used for $\{\boldsymbol{a}\}$,

$$\{\boldsymbol{t}\} = [\boldsymbol{P}][\boldsymbol{S}]^{-1}\ \{\tilde{\boldsymbol{u}}\} = [\boldsymbol{K}]\{\tilde{\boldsymbol{u}}\} \tag{16}$$

where $[\boldsymbol{K}]_{(4\times4)}$ is the dynamic stiffness matrix, which relates nodal surface tractions to the nodal displacements. Note that the preceding stiffness matrix is to be formed and Eq. (16) is to be solved for each value of ω_n and η_m.

Throwoff Element

One of the characteristic problems in wave propagation is analyzing infinite or semi-infinite structures when one or all of the boundaries lie at infinity. This geometry can be modeled in SE with great ease. The element is also equivalent to simulating absorbing boundary conditions or adding maximum damping to the structure. Such an element, which is essentially single noded, can be formulated by setting the layer depth $L \to \infty$. This necessarily implies that there will not be any reflection coming from the second node in a finite duration of time, which means only forward-propagating parts of the waves are to be considered. The displacement field in this case can be written as

$$\hat{u}(x) = R_{11}Ae^{-jk_1x} + R_{12}Be^{-jk_2x}$$

$$\hat{v}(x) = R_{21}Ae^{-jk_1x} + R_{22}Be^{-jk_2x} \tag{17}$$

A and B again can be written in terms of nodal displacements of node 1, u_1 and v_1, as

$$\{\boldsymbol{a}\} = [\boldsymbol{S}]^{-1}\{\tilde{\boldsymbol{u}}\} \tag{18}$$

where $\{\boldsymbol{a}\} = \{A, B\}^T$, and $\{\tilde{\boldsymbol{u}}\} = \{u_1, v_1\}^T$. The matrix of coordinate transformation $[\boldsymbol{S}]$ is given by

$$\boldsymbol{S} = \begin{bmatrix} R_{11} & R_{12} \\ R_{21} & R_{22} \end{bmatrix} \tag{19}$$

The tractions at node 1 can be related to displacements of node 1, as done before. The relation yields the same Eq. (15), where elements of $[\boldsymbol{P}]$ are $(p = 1, 2)$

$$P_{1p} = j(2\mu + \lambda)R_{1p}k_p - \lambda\eta R_{2p}$$

$$P_{2p} = -\mu(-jR_{2p}k_p - \eta R_{1p}) \tag{20}$$

and $[\boldsymbol{K}]_{(2\times2)}$ is the dynamic stiffness matrix for this element.

When the wave numbers come in pairs (if only even orders are present in the polynomial of k), it is possible to discriminate between forward and backward propagating terms (positive and negative parts). In the present case, all four roots can be different, and conjugateness between them may be absent for a wide range of frequencies. In such a case, special care needs to be taken to choose the wave numbers. Here, the first wave number is fixed as the first element of the array that is coming out of the equation solver. The second wave number has the property that the basis vector of the null space of wave matrix corresponding to this wave number will be linearly independent of the basis vector of the null space of the wave matrix corresponding to the first wave number, that is, $[\boldsymbol{R}]$ will have rank 2. The second wave number is chosen based on certain criteria. First, we search for the wave number that has largest distance from the first wave number (with respect to the usual norm of C^2). This algorithm successfully captures the correct wave number when the roots are complex conjugates. However, when the roots are not complex conjugate and are very close to each other, this algorithm fails to recognize the correct wave number. In such cases, an alternate algorithm is used. Here, after forming all possible combinations of $[\boldsymbol{R}]$ matrices (first column fixed), they are checked for their singularity in terms of determinants and singular values. The most suitable candidate is the one that has a nonzero determinant and the lowest singular value.

When all of these criteria are fulfilled, the singlenoded element performs very well irrespective of the conjugate/nonconjugate wave numbers, which is shown in next numerical experiment section. These algorithms make the solver robust and efficient against all numerical instabilities that are common in all frequency-domain methods.

Spectral and Temporal Windows

Because the summations are finite in the expression of u and v, there is a window associated with each: one in time of duration T and one in space with length Y. The increments of wave number $\Delta\eta$ and the frequency $\Delta\omega$ are related to the window length and sampling by the relations

$$\Delta\eta = 2\pi/Y = 2\pi/(M\Delta y), \qquad \Delta\omega = 2\pi/T = 2\pi/(N\Delta t)$$

where Δy and Δt are spatial and temporal sampling, respectively. As a consequence of the finite summation, the reconstructions are periodic over time and space windows. Therefore, it is necessary to ensure that waves from neighboring space windows have negligible amplitudes by the time they reach the observation window. This is accomplished by choosing a sufficiently large space window. The effect of the neighboring window is further diminished by damping. Further discussion on these issues is given by Doyle.[16]

Boundary Conditions

The boundary conditions are implemented by the usual partitioning of the system matrices. For free boundary conditions, tractions T_{xn} and T_{yn} will be zero at node n. The loaded boundary conditions (symmetric) at node n become

$$t_{x,y\,n} = S(y)F(t) = \left[\frac{a_0}{2} + a_m \cos(\eta_m y)\right]\left[\sum_{n=0}^{N-1} \hat{F}_n e^{-j\omega_n t}\right] \quad (21)$$

where $S(y)$ is an even spatial variation of the load having the Fourier coefficients a_m and $F(t)$ is the time variation of the load with the Fourier coefficients $\hat{F}_n$.

Effect of Temperature

If the temperature of the layer is increased by ΔT degrees centigrade, the thermal strains generated are $\varepsilon_{xx} = -\alpha_x \Delta T$ and $\varepsilon_{yy} = -\alpha_y \Delta T$, where α_x and α_y may vary spatially. These strains, in turn, generate thermal stress of which only the σ_{xx} component is of interest and is given by $\sigma_{xx} = -\{(\lambda + 2\mu)\alpha_x + \lambda\alpha_y\}\Delta T = -\Theta\Delta T$. If it is assumed that the temperature ΔT does not vary with spatial coordinates, then there are no extra terms in the governing differential equation. However, the specification of natural boundary conditions will change at the layer interface. Equation (13) will be modified as

$$T_{x1} = -T_{11}(0) + \Theta(0)\Delta T, \qquad T_{x2} = T_{11}(L) - \Theta(L)\Delta T$$
$$T_{y1} = -T_{12}(0), \qquad T_{y2} = T_{12}(L) \quad (22)$$

Hence, the equilibrium equation will be modified as $\{\boldsymbol{t}\} = [\boldsymbol{P}][\boldsymbol{S}]^{-1}\{\tilde{\boldsymbol{u}}\} + \{\tilde{f}\} = [\boldsymbol{K}]\{\tilde{\boldsymbol{u}}\} + \{f\}$.

Here $\{\tilde{f}\}$ is the thermal load vector given by

$$\{\tilde{f}\} = \{\Theta(0)\Delta T \quad 0 \quad -\Theta(L)\Delta T \quad 0\}^t$$

Hence, along with mechanical load vector, an extra load vector will arise because of thermal load, where the load is essentially tensile or compressive (no shear component).

Numerical Experiments

In this section, the detailed procedure of force identification is given. First, the present element is validated by comparing its response with the response of a two-dimensional FE analysis. In FE analysis, the inhomogeneous material is modeled by interpolating material properties within an element using the same shape functions that describe displacements. Once the validation is over, the smoothening effect of the FGM is studied. Next, the effect of thermal burst loading is investigated. Finally, the present element and FE meshes are employed to reconstruct an applied force history.

Validation

To magnify the effect of nonhomogeneity, an all-FGM two-dimensional layered media of unit thickness is considered (Fig. 2). The layer has a dimension of 0.5 m in the X direction and 1.0 m in the Y direction. The bottom of the layer is assumed fixed. Material properties vary smoothly from that of steel at the topmost layer to that of ceramic at the bottommost layer. For ceramic, the material properties are $E = 390$ GPa, $\nu = 0.3$, and $\rho = 3950$ kg/m^3. Similarly, for steel, $E = 210$ GPa, $\nu = 0.3$, and $\rho = 7800$ kg/m^3. For these material properties, inhomogeneous parameters α, β, and γ become 1.7143, 1.4250, and -0.9872, respectively. These material properties along with 0.5-m element depth generate a wave number distribution over frequencies (for $\eta_m = 20$) as shown in Fig. 3. As is seen in Fig. 3, there are two cut-off frequencies (frequencies where wave numbers are zero) before which wave numbers were imaginary and, hence, not propagating. Although Fig. 3 suggests that wave numbers are complex conjugate to each other, in reality they are slightly perturbed from the conjugate roots. This perturbation comes from nonzero values of the coefficients of k and k^3 in the spectrum relation, as discussed earlier. In one dimension, a single SE is sufficient to model a regular structure of any length. Even in two dimensions, for isotropic homogeneous material, a single element will model a layer of any depth. However, because the present element is not exact (because the spectrum relation is not satisfied exactly), one element will not suffice to model an inhomogeneous layer. Instead, three SE are used here to model this media.

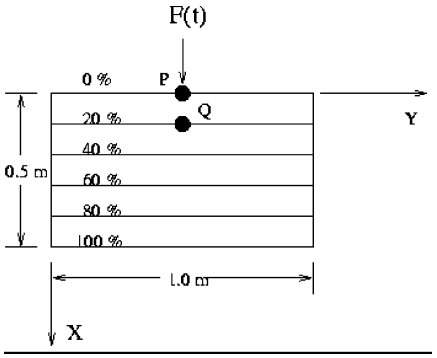

Fig. 2 Two-dimensional layered media model for analysis; percentage indicates ceramic content.

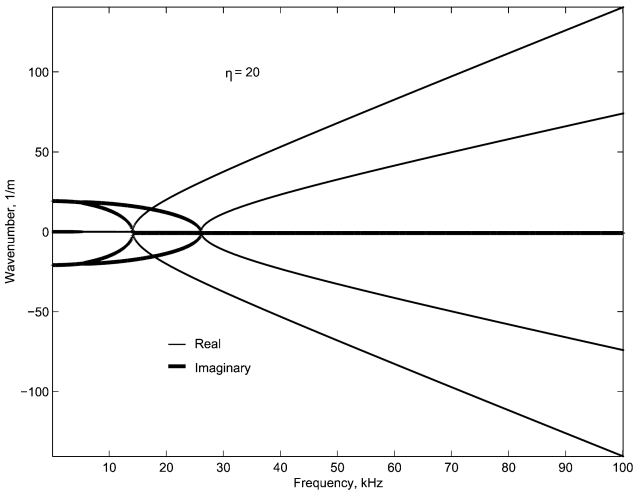

Fig. 3 Wave number of model in verification study.

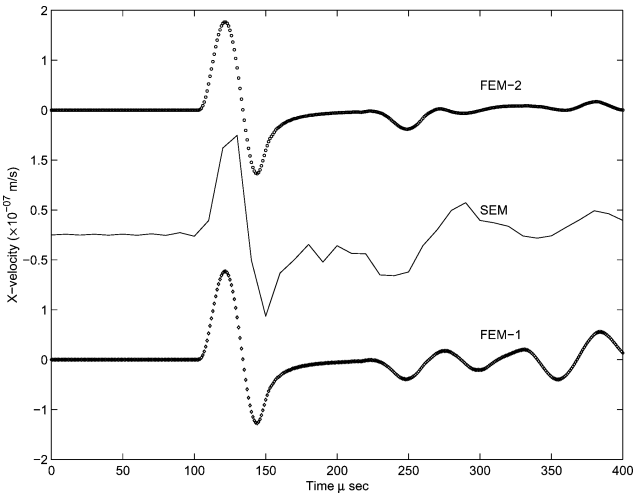

Fig. 5 Verification of present element.

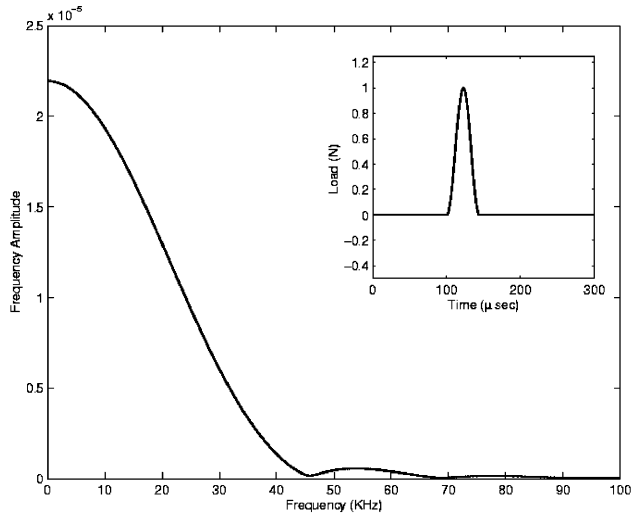

Fig. 4 Spectrum of the mechanical load; inset, time history.

For FE analysis, two meshes are considered. In the first mesh, length of the layer in Y direction is taken to be 1.0 m and depth is 0.5 m, as is the layer size. The domain is modeled with 1800 plane strain triangular FEs. In the second mesh, the length of the layer is taken as 2.0 m, with the same depth. The domain is modeled with 7200 plane strain triangular FEs. The purpose of this mesh is to highlight the reflections coming from the boundaries being normal in the Y direction, which the present SE cannot capture. These two meshes and the results obtained from them will be referred to as FEM-1 and FEM-2, respectively. At this point, the efficiency of the SE can be reiterated by comparing the system sizes of the global matrices obtained in different meshes. The matrices are described by number of rows (number of equations) and half-bandwidth. In FEM-1, the system size is 3656×126, and in FEM-2, the system size is 7258×148. In comparison, the SE system size is 6×3. Thus, the SE system size is very nominal compared to FE system sizes.

An impulse load is applied at the midpoint of the top surface of the inhomogeneous layer (marked by P), as shown in Fig. 2. The load has frequency content of about 46 kHz and duration of 50 μs (Fig. 4). Response of the layer (X velocity) at point Q (which is 0.05 m away from P) predicted by the present element is shown in Fig. 5. The result is compared with results obtained from the FE analyses of the meshes FEM-1 and FEM-2.

As is shown in Fig. 4, the response predicted by the present element has good agreement with that of FEM-1 and FEM-2. The magnitude of the initial response is reported quite accurately in SE. In the present SE, inhomogeneity is introduced by the approximate wave number and consideration of the material property variation while evaluating surface tractions. These two considerations are not sufficient to predict the propagating speed of the P and S waves in inhomogeneous material. For this kind of loading, the wave propagates as a P wave in the layer. The FEM-1 and FEM-2 responses show an inverted peak at around 225 μs, which is the reflection of the P wave from the fixed edge at the bottom of the layer. This reflection comes a little earlier in the SE response, which indicates that P wave speed in the SE model is higher than the actual (FE response). Furthermore, FEM-1 shows several reflections that are missing in both FEM-2 and SE responses. These are the reflections coming from the free edges of the layer. In SE, there is no free edge, and in FEM-2, the edge is at sufficient distance so that reflections do not enter in the time window. Similarly, reflections present in FEM-1 are absent in SE responses. Thus, the FEM-2 helps in isolating the reflections coming from the free edges. Other than the absence of these reflections, the SE captures the behavior of the inhomogeneous layer quite accurately in terms of magnitude of the response. This analysis shows that the present element is suitable for wave propagation analysis of inhomogeneous materials in terms of both accuracy and efficiency.

Smoothening by FGM

Because FGM smoothly blends the properties of the two base materials, it is expected that the stress/strain jump that exists in the bimaterial layer interface will disappear (or at least reduce) when the FGM layer is introduced. To ascertain this, a layered structure of two base materials, steel and ceramic, is taken for the study. In the first model, these two materials are fused together without any FGM layer in between. The depth of each layer is taken as 0.5 m. Material properties of steel and ceramic are as taken before. In the second model, an FGM layer is introduced in between the base materials. The thickness of each material is halved, and the thickness of the FGM material, thus, becomes 0.5 m. Because the material properties in FGM vary from steel to ceramic (within 0.5 m), the inhomogeneous parameters α, β, and γ have the same values as obtained before. The same pulse load, which is applied in the earlier model, is applied here on the steel surface in the X direction. The X directional velocity at $x = 0.5$ m (material interface for model 1 and mid-FGM layer for model 2) is shown in Fig. 6. As seen in Fig. 6, the response of the second model displays several features that are absent in its model 1 counterpart. The initial amplitude of the response of model 2 is less than that of model 1 (point in the graph marked 0). Furthermore, FGM successfully reduces the amplitude of the reflected pulses at the points 1′, 1, 2, 3, 4, 5, and 6 in Fig. 6.

Next, the strain E_{11} and stress T_{11} variation at the same location, $x = 0.5$ m, is plotted in Figs. 7 and 8. As in Fig. 7, the strain measured in the layer interface is quite different in the steel and the ceramic sides. The difference in the initial peak strain is quite high (more than double, as shown at point 0), and subsequently, this

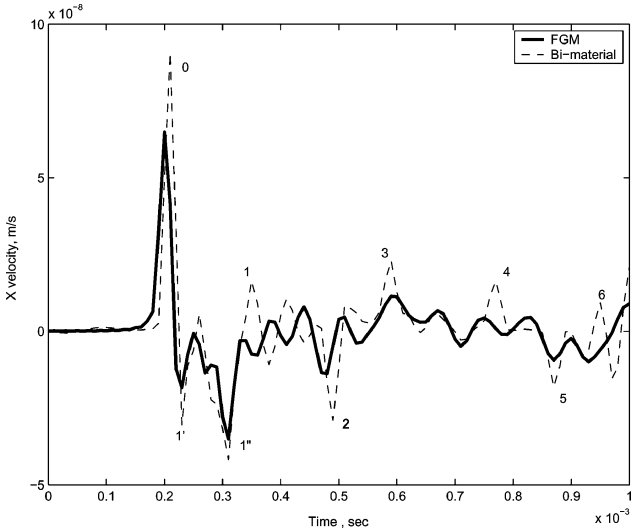

Fig. 6 Smoothening effect of FGM; X velocity history.

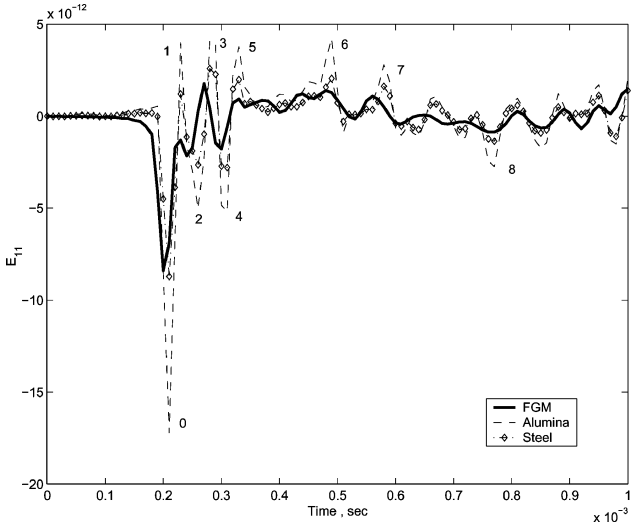

Fig. 7 Smoothening effect of FGM; strain variation.

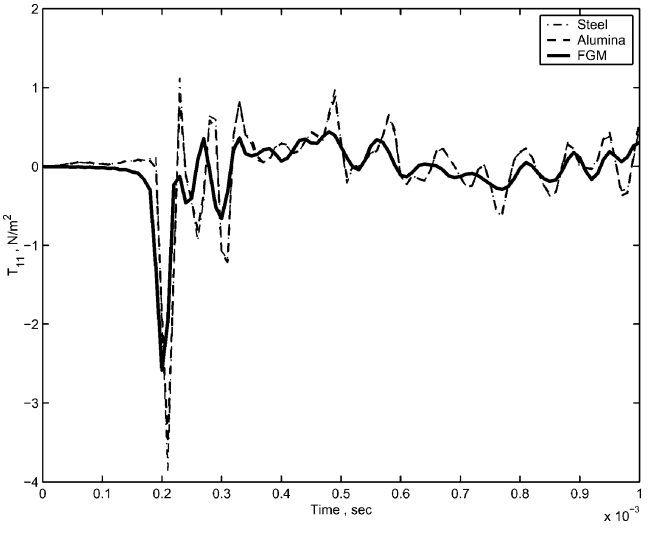

Fig. 8 Smoothening effect of FGM: stress variation: ——, FGM layer and ·–·–·– and – – – –, bimaterial layer.

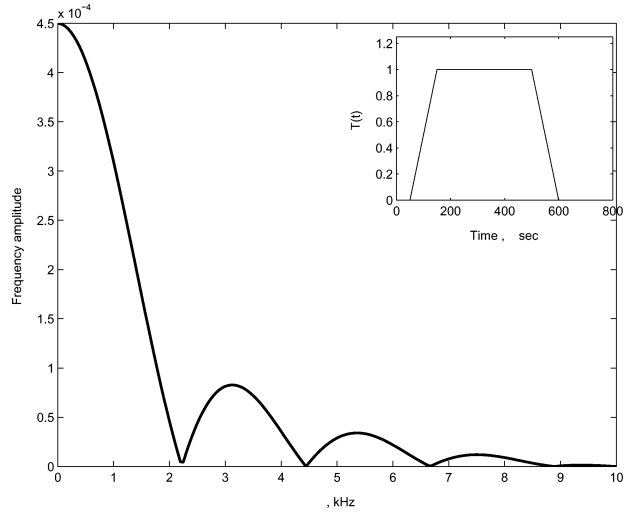

Fig. 9 Spectrum of temperature variation; inset, time-domain input.

difference is reduced. This jump in strain is quite expected because the strain–displacement matrix $\boldsymbol{B}$ is different for the two materials. However, introduction of the FGM layer greatly reduces the peak strain (making it closer to that predicted in steel layer), and all of the other points, points 1–8, consecutively, FGM predicts the lowest strain response. The stress variation is shown in Fig. 8. Unlike the strain variation, the stress history does not show any jump at the interface because the continuity of the stress (tractions) is imposed at the nodes. Otherwise, the variations for FGM, metal, and ceramic follow the same pattern as is seen in the strain response. Most important, FGM smoothens the stresses in all of the crucial points.

Effect of Thermal Load

As discussed before, thermal stress plays an important role in the FGM microstructure because of the mismatch in the thermal expansion coefficients of the base materials. Here, a ceramic–FGM–steel layer is taken to study the effect of thermal burst loading. In the top of the layer, there is ceramic of 0.25 m thickness, then the FGM layer of 0.5 m thickness, which smoothly blends the property of ceramic to that of steel, which is again 0.25 m thick. Metal and ceramic material properties are as taken before. However, values of the inhomogeneous parameters are different in this case because FGM transcends from ceramic to steel, rather than steel to ceramic, as before. It is assumed that the coefficients of thermal expansion α_x and α_y are equal for both ceramic and steel and that their values are $7.0E-06/^\circ$C and $14.0E-06/^\circ$C, respectively. In this case, the inhomogeneous parameters α, β, and γ have the values -0.9231, -0.9231, and 1.9494, respectively. The ceramic layer is suddenly heated by a ramp kind of temperature variation, shown in Fig. 9. As is shown in the inset of Fig. 9, the temperature builds up in 100 μs, remains in the peak value up to 500 μs, and decreases in the same fashion. Frequency-domain representation of this load is also shown in Fig. 9 (which will be fed to the SE solver), which shows that the load has comparatively low-frequency content (of about 2 kHz). Because of this thermal loading, the X directional velocities of different points in the layer are plotted in Fig.10. The responses at around 50 μs denote the effect of the rising leg of the load. Note that the wave propagates only when there is a change in magnitude of the input pulse (in the time domain). Thus, the constant part of the load actuates no wave. The top surface of the ceramic experiences the maximum amplitude of velocity and the magnitude decreases as one goes away from the ceramic layer to steel layer. The inverted waveforms at around 500 μs denote the effect of the falling leg of the load.

As deduced earlier, effect of temperature rise/fall is solely manifested in normal traction, and this stress at several locations of the layer is measured and shown in Fig.11. As seen from Fig. 11, the top surface of the ceramic layer is subjected to maximum compressive stress (around 80 MPa) and the ceramic FGM interface is subjected to maximum tensile stress (around 20 MPa). However, quite a

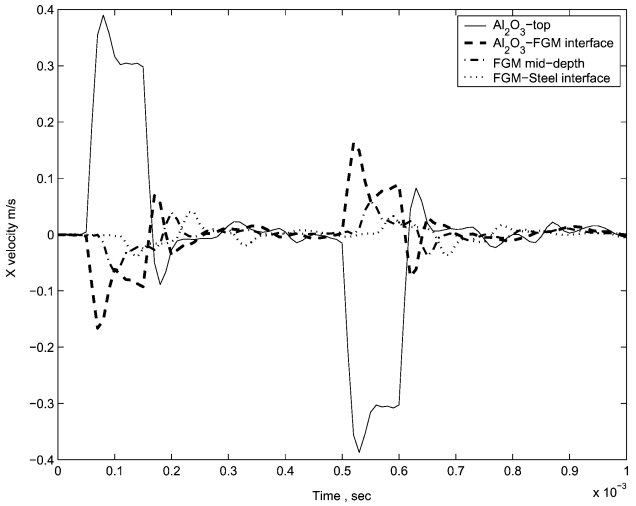

Fig. 10 Response to thermal shock; *X* velocity history.

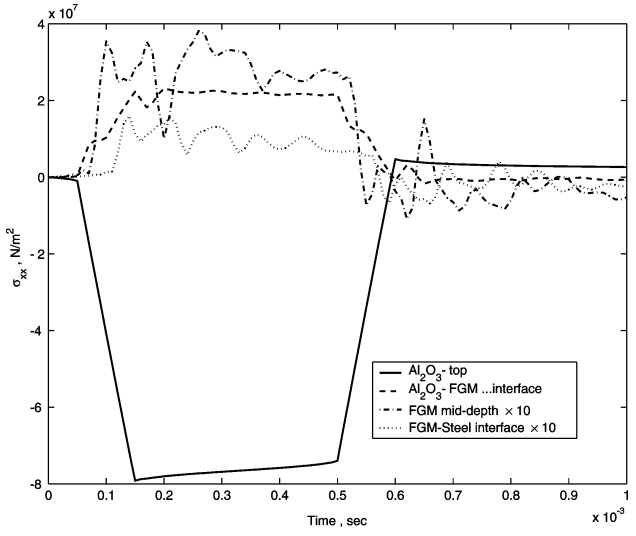

Fig. 11 Response due to thermal shock; stress history.

nominal amount of stress is transmitted through the FGM layer as the stresses at mid-FGM layer and FGM-steel interface suggest. (They are magnified 10 times in Fig. 11.) Contrary to the velocity plot, the stress plot reiterates the presence of load up to around 600 μs.

Force Identification

The basic idea of force identification in frequency-domain analysis is presented next. Because the whole spectral formulation is in the frequency/wave number domain, the response is related to the input through the transfer function in the frequency/wave number domain as

$$\hat{\boldsymbol{Y}}(\omega_n, \eta_m) = \tilde{\boldsymbol{H}}(\omega_n, \eta_m)\hat{\boldsymbol{X}}(\omega_n, \eta_m) \tag{23}$$

where $\hat{\boldsymbol{X}}(\omega_n, \eta_m)$ is the transformation of the input; for example, load, $\hat{\boldsymbol{Y}}(\omega_n, \eta_m)$ is the transform of the output (typically, velocity, strain, etc.), and $\tilde{\boldsymbol{H}}(\omega_n, \eta_m)$ is the system transfer function. Now, input force can be obtained easily by dividing the transform of the response by the transfer function, that is,

$$\hat{\boldsymbol{X}}(\omega_n, \eta_m) = \hat{\boldsymbol{Y}}(\omega_n, \eta_m)/\tilde{\boldsymbol{H}}(\omega_n, \eta_m) \tag{24}$$

Thus, if the response is known at some point, then the disturbance that caused it can be computed. This is one of the distinct advantages of the spectral approach in its ability to solve inverse problems. In general, $\hat{\boldsymbol{Y}}(\omega_n, \eta_m)$ will be experimental data, typically transform of strain history.[10] In this work, FE analysis output is taken as replacement of experimental output, and these data are fed into the spectral solver to reconstruct the force history. The experimental outputs are always truncated at some point. This is the reason why the FE output is also truncated to simulate the experimental environment. Because the main purpose is to reconstruct the pulse kind of loading, it is essential to take only the initial portion of the history (where the pulse load is manifested first), and the reflection from the boundary (where the load is replicated) should be excluded. This is necessary because the present element is infinite in the y direction. In this way, the effect of boundary is eliminated and the applicability of the system increases. The present problem is a second-order system, where in most cases, the waves are nondispersive in nature. The tracking of reflection is quite trivial in such systems.

Details of the numerical experiment for force identification are outlined next. The geometry, material distribution, load, point of application, boundary conditions, and number of elements for FE meshes and SE mesh remain the same as before. The FE responses (velocity in the *X* direction) FEM-1 and FEM-2 are truncated at various points in time. These truncated responses are then transformed into the frequency domain and fed to the SE solver for inverse analysis. Both responses FEM-1 and FEM-2 are employed to reconstruct the force history. Although, FEM-2 mesh does not conform to the exact layer dimensions, nevertheless it is instrumental in isolating the effect of the reflections from boundary. The truncated responses at various points in time axis for FEM-1 and FEM-2 are shown in Fig. 12. The solid line denotes FEM-1 response, and dashed line denotes FEM-2 response. As seen in Fig. 12, both FEM-1 and FEM-2 generate same response if truncated at 225 μs. However, for responses truncated at 500 and 1000 μs, there is considerable difference between FEM-1 and FEM-2 responses. Hence, it is expected that they will reconstruct different load histories. First, the force reconstructed from FEM-1 response is shown in Fig. 13. As seen in Fig. 13, the magnitude of the load is predicted correctly by all three truncated responses. There is a peak at around 225 μs in the reconstructed force history, which is absent in the original force history. This peak is due to mismatch in the reflected pulse of FE responses and SE response, which was discussed earlier. Furthermore, the forces reconstructed by truncated responses at 1000 and 500 μs show another unwanted reflection at around 350 μs, which is because of the reflections from the free edges. This reflection is absent in the force reconstructed from the responses truncated at 250 and 200 μs because there is no reflection (from free edges) in these truncated responses. Furthermore, these are the optimum truncated responses for this particular FE model.

The FE model of FEM-2 has a larger dimension in the *Y* direction, and because of that, there is less reflection from the free edge compared to the FEM-1 response. There is no other difference between FEM-1 and FEM-2 responses, and the magnitudes are same. Hence, it can be expected that FEM-2 will generate a clearer reconstructed

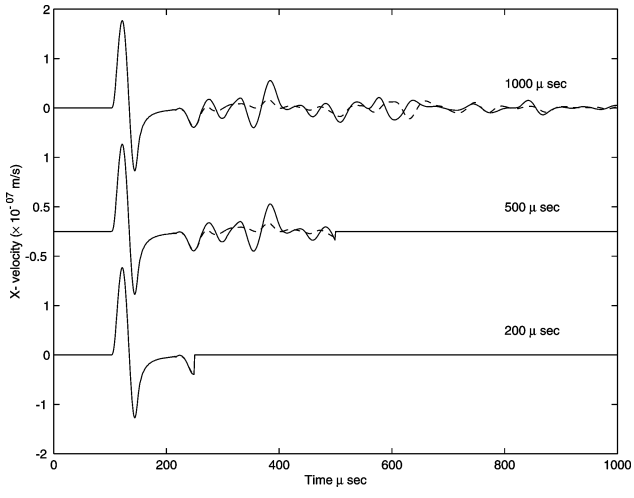

Fig. 12 Various truncated responses of FE output.

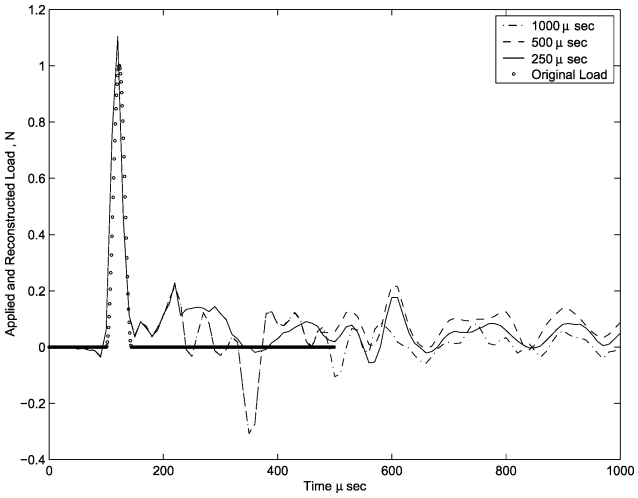

Fig. 13 Force reconstruction by SE analysis; legend indicates truncation point.

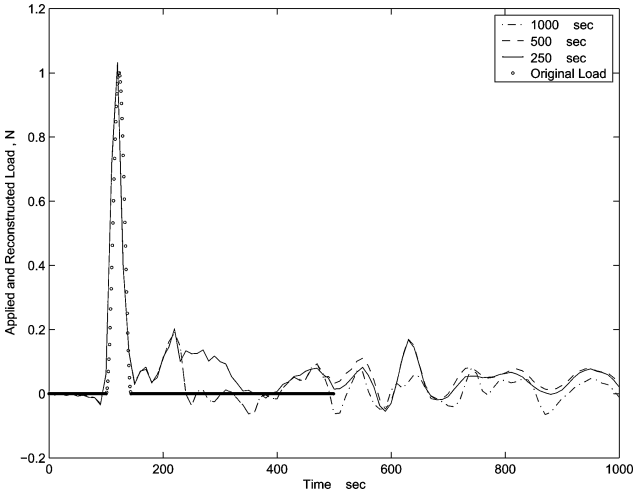

Fig. 14 Force reconstruction by SE analysis; legend indicates truncation point.

force for all truncated responses. Figure 14 shows the force histories generated for different truncated responses of FEM-2. As seen in Fig. 14, all of the truncated responses predict the initial pulse quite accurately and they are devoid of any reflection like that of FEM-1 reconstructions. This fact reiterates the need for proper choice of truncation points in the experimental measured responses, which depends on the geometry of the structure. This example shows that if the truncation point is less than about 250 μs, a comparable force history can be reconstructed. Overall, the example shows the efficiency of the SE method in force identification.

Conclusions

A two-noded approximate-layered spectral element is developed to analyze inhomogeneous media subjected to high-frequency impact loading. It is assumed that material properties, such as elastic modulus and density, are varying linearly along a spatial direction. The governing equations for this kind of material are PDEs with variable coefficients. When the method of integral transforms is applied to these equations, a set of ODEs are obtained, which again has variable coefficients. Thus, it is not possible to obtain the exact solutions of these ODEs, which hitherto provided the backbone of SE formulation. In this work, it is assumed that exact solution to the governing equations of homogeneous materials is still applicable for inhomogeneous materials. This assumption generates a new spectrum relation and, ultimately, a new SE where the effects of nonhomogeneity are embedded. Although the element is not exact as are its predecessors, when the degree nonhomogeneity is small (in terms of α, β, and γ), a few elements are sufficient to model a layer, which greatly reduces the cost of computation.

The element predicts the response of an inhomogeneous structure with no amplitude error, although there remains small period error (manifested in the time of arrival of reflected pulses). For the fundamental application of FGM in mitigating stress jump at a bimaterial interface, it is shown that the formulated element can capture the smoothing effect of FGM. It is found that FGM reduces not only the peak amplitude of the response but also the magnitude of the reflected waveforms. Other than the effect on mechanical response for bimaterials, FGM also plays important roles for response due to thermal loading. This is brought out in an example in which FGM blends the mismatch in the coefficient of thermal expansion. The example illustrates the effect of FGM in thermal barrier coating where most of the high-thermal stresses exist in the ceramic layer and in the ceramic–FGM interface, and this magnitude decreases in the other side of the graded material.

Frequency-domain formulation of SE has an added advantage in solving inverse problems of force identification, which is investigated in the final example. As a replacement of experimental data, a truncated FE analysis output of an inhomogeneous structure subjected to high-frequency impact loading is considered. This impact load is estimated by SE model of the same structure. It is shown that the force can be reconstructed without any period or magnitude error. Also, associated with every configuration, there is one optimal point of truncation that will yield the most accurate reconstructed force histories. This may obviate the difficulties of performing tedious experiments where other problems such as noise, improper data acquisition, etc., are associated.

References

[1]Caviglia, G., and Morra, A., *Inhomogeneous Waves in Solids and Fluids*, World Scientific, Singapore, 1992, pp. 1–5.

[2]Poiree, B., "Complex Harmonic Plane Waves," *Physical Acoustics*, edited by O. Leroy and M. A. Breazeale, Plenum, New York, 1991.

[3]Liu, G. R., Tani, J., and Ohyoshi, T., "Lamb Waves in Functionally Gradient Material Plates and Its Transient Response, Part I: Theory," *Transactions of Japan Society of Mechanical Engineers*, Vol. 57A, No. 535, 1991, pp. 603–608.

[4]Liu, G. R., Tani, J., and Ohyoshi, T., "Lamb Waves in Functionally Gradient Material Plates and Its Transient Response, Part II: Calculation Results," *Transactions of Japan Society of Mechanical Engineers*, Vol. 57A, No. 535, 1991, pp. 609–611.

[5]Liu, G. R., and Tani, J., "SH Surface Waves in Functionally Gradient Piezoelectric Material Plates," *Transactions of the Japan Society of Mechanical Engineers*, Vol. 58A, No. 547, 1992, pp. 504–507.

[6]Liu, G. R., and Tani, J., "Surface Waves in Functionally Gradient Piezoelectric Plates," *Journal of Vibration and Acoustics*, Vol. 116, 1994, pp. 440–448.

[7]Reddy, J. N., and Chin, C. D., "Thermo-Mechanical Analysis of Functionally Graded Cylinders and Plates," *Journal of Thermal Stresses*, Vol. 26, No. 1, 1998, pp. 593–626.

[8]Praveen, G. N., and Reddy, J. N., "Nonlinear Transient Thermo-Elastic Analysis of Functionally Graded Ceramic-Metal Plates," *International Journal of Solids and Structures*, Vol. 35, No. 33, 1998, pp. 4457–4476.

[9]Gong, S. W., Lam, K. Y., and Reddy, J. N., "The Elastic Response of Functionally Graded Cylindrical Shells to Low Velocity Impact," *International Journal of Impact Engineering*, Vol. 22, No. 4, 1999, pp. 397–417.

[10]Han, X., Liu, G. R., and Lam, K. Y., "Transient Waves in Plates of Functionally Graded Materials," *International Journal of Numerical Methods in Engineering*, Vol. 52, No. 8, 2001, pp. 851–865.

[11]Han, X., Liu, G. R., Xi, Z. C., and Lam, K. Y., "Transient Waves in a Functionally Graded Cylinder," *International Journal of Solids and Structures*, Vol. 38, No. 17, 2001, pp. 3021–3037.

[12]Han, X., Liu, G. R., Xi, Z. C., and Lam, K. Y., "Characteristics of Waves in Functionally Graded Cylinder," *International Journal of Numerical Methods in Engineering*, Vol. 53, No. 3, 2002, pp. 653–676.

[13]Chakraborty, A., Gopalakrishnan, S., and Reddy, J. N., "A New Beam Finite Element for the Analysis of Functionally Graded Materials," *International Journal of Mechanical Sciences*, Vol. 45, No. 3, 2003, pp. 519–539.

[14]Chakraborty, A., and Gopalakrishnan, S., "A Spectrally Formulated Finite Element for Wave Propagation Analysis of Functionally Graded Beams," *International Journal of Solids and Structures*, Vol. 40, No. 10, 2003, pp. 2421–2448.

[15]Chakraborty, A., and Gopalakrishnan, S., "Various Numerical Techniques for Analysis of Longitudinal Wave Propagation in Inhomogeneous One-Dimensional Wave-Guides," *Acta Mechanica*, Vol. 162, No. 1-4, 2003, pp. 1–27.

[16]Doyle, J. F., *Wave Propagation in Structures*, Springer-Verlag, New York, 1997.

[17]Rizzi, S. A., and Doyle, J. F., *Force Identification for Impact of a Layered System, Computational Aspects of Contact, Impact and Penetration*, Elmepress International, Lausanne, Switzerland, 1991, pp. 222–241.

[18]Han, X., and Liu, G. R., "Effects of SH Waves in a Functionally Graded Plate," *Mechanics Research Communication*, Vol. 29, No. 5, 2003, pp. 327–338.

[19]Berezovski, A., Engelbrecht, J., and Maugin, G. A., "Numerical Simulation of Two-Dimensional Wave Propagation in Functionally Graded Materials," *European Journal of Mechanics—A/Solids*, Vol. 22, No. 2, 2003, pp. 257–265.

[20]Markworth, A. J., Ramesh, K. S., and Parks, W. P., Jr., "Modeling Studies Applied to Functionally Graded Materials," *Journal of Materials Science*, Vol. 30, No. 9, 1995, pp. 2183–2193.

[21]Doyle, J. F., "Further Developments in Determining the Dynamic Contact Law," *Experimental Mechanics*, Vol. 24, No. 4, 1984, pp. 265–270.

[22]Doyle, J. F., "Force Identifications from Dynamic Response of a Bi-Material Beam, *Experimental Mechanics*, Vol. 33, No. 1, 1993, pp. 64–69.

[23]Doyle, J. F., "Determining the Contact Force During the Transverse Impact of Plates," *Experimental Mechanics*, Vol. 27, No. 1, 1987, pp. 68–72.

[24]Doyle, J. F., "Experimentally Determining the Contact Force During the Transverse Impact of Ortho-Tropic Plates," *Journal of Sound and Vibration*, Vol. 118, No. 3, 1987, pp. 441–448.

K. Shivakumar
Associate Editor